Final Report for Period: 01/01/2008 – 12/31/2008 **Submitted**: 7/27/2009

Investigator Samuel B. French (PI) **Award ID**: 0741195

Investigator Robert Dean (Co-PI)

Firm: MEMSense, LLC, 2693D Commerce RD. Rapid City, SD 57702 (605) 342-2553

Title: Application of an Electrostatic Actuator Stable-Range-of-Motion Enhancement Control Law to Improve MEMS Gyroscopic Sensors.

MEMSense Investigators and Personnel

Samuel B. French, Research Scientist, MEMSense, LLC.

sfrenchg@memsense.com

Mike Gibson, Senior Firmware Engineer, MEMSense, LLC.

mgibson@memsense.com,

James P. Brunsch, CTO, Senior Electronics Engineer, MEMSense, LLC.

jbrunsch@memsense.com

Auburn University Investigators and Faculty

Robert N. Dean, Assistant Professor, Dept. of Electrical and Computer Engineering, Auburn. University.

rdean@eng.auburn.edu

John Hung, Professor, Dept. of Electrical and Computer Engineering, Auburn University.

hungjoh@auburn.edu

Fa Foster Dai, Professor, Dept. of Electrical and Computer Engineering, Auburn University.

fosterdai@auburn.edu

Auburn University Staff

Charles Ellis, Electrical Engineering Dept, Auburn University.

Graduate Students

Joseph Cali

Ryan McPherson

Aditi Rane

Colin Stevens

Seong Jin Kim,

Kun-Tao Chung

Bill Souder

Phil Reiner

1.0 Summary of Technology

1.1 Gap-Closing Actuators and Performance Enhancement

MEMSense has development a number of inertial sensors based on micro electromechanical systems (MEMS) that make use of gap closing actuators. This particular actuator type is used for several reasons, of which the most important is the magnitude of the capacitance that can be developed on the movable structure given a corresponding voltage. Capacitance associated with the actuator must be as large as possible to ensure that signals can be resolved in the presence of electrical and mechanical noise. Also of importance is that the actuator should have the greatest range-of-motion between the equilibrium point and the fixed plate. Without significant relative range-of-motion it is difficult to construct a practical device without increasing overall size of the MEMS device significantly. Many MEMSense customers are seeking even smaller devise so that access to inertial information can be available in new application never possible before. Great opportunity lies in the use of gap closing actuators with better linear response to make inertial measurement devices as small as possible while increasing precision. A parallel plate capacitor (Figure 1) represents the simplest implementation of a gap closing actuator (GCA). The goal of these investigations was to establish the benefits of adding a series capacitance (SCM) to this system in combination with synthetic voltage division (SVD) methods in increasing linearity in gap closing actuators. Specifically, those actuators in the form of interdigitated comb drives (**Error! Reference source not found.**) were studied due to their relevance to gyroscopes being developed by MEMSense. The SCM and SVD concepts were proven on theoretical grounds via computer modeling, as well as in laboratory trials consisting of combined MEMS element and control electronics fabricated as part of this effort. These results have great applicability to the novel gyroscope designs currently being developed at MEMSense.

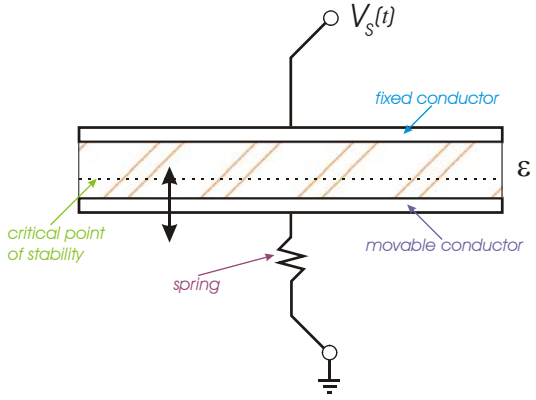

Figure 1: Parallel Plate Capacitor Actuator

2.0 Activities and Findings

2.1 Feasibility of the current GCA design

MEMSense has been actively developing sensors that make use of GCA elements for dynamic control (“driving”) and sensing functions. The main benefit of MEMS devices utilizing these structures are high capacitance change per unit displacement which leads to good sensitivity in inertial sensors. Maintaining sufficient capacitance per unit volt

that is available is vitally important, and this makes GCA an obvious choice. The main drawback in using GCA elements is the limitations imposed by the nonlinear behavior in the capacitance versus voltage of this configuration which works against miniaturization of the system. In the limiting case of a bare parallel plate actuator, a maximum displacement of less than one third of the total gap between plates must be maintained due to instability encountered at that point. It was found that the SVD and SCM elements sufficiently linearize the response of GCAs and MEMSense will take full advantage of these methods to increase the performance of devices relying on GCA elements for operation.

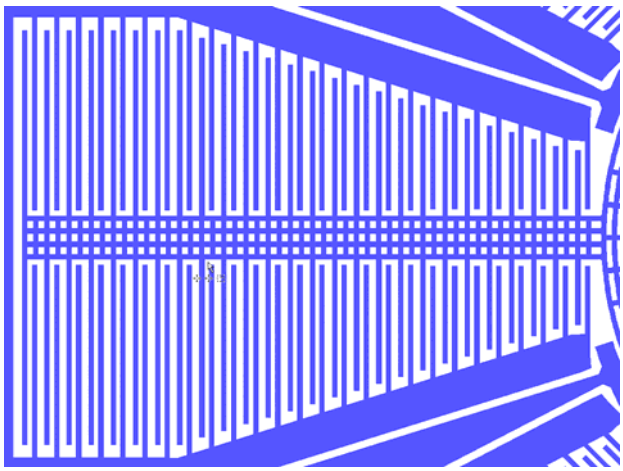

Figure 2: MEMSense GCA Element

2.2 The MEMSense GCA

A typical GCA in the current MEMSense designs take on some unusual shapes such as the device that contains truncated combs as seen in **Error! Reference source not found.**. These devices have been designed out of the requirement that the maximum displacement, the range-of-motion, of the movable structures is to be kept much smaller than the gap width (x<<5% of the gap). This must be done in order to maintain an approximate linear behavior since the movable structure is under the influence of forces that are nonlinear with displacement, analogous to those forces of the parallel plate. In an effort to maintain sufficient capacitance the GCA elements are made as large as possible resulting in device packaged devices that are larger than comparable gyroscope technologies.

2.3 Testable GCA Design and Fabrication

A GCA was designed (Two models were developed one in the Simulink environment and another model in PSpice to test the combined GCA, series capacitance, and synthetic voltage division system.

2.5.1 Simulink Simulations

A simulation was conducted with a mathematical representation of the GCA with the addition of a series capacitance and the SVD controller. A nominal value of 1pF for the series capacitance, with a system gain K =48 for the controller, was chosen to establish a baseline response of the system. The resulting controller input voltage, V_{in} / K, and the resulting voltage across the actuator was determined for various values (**Error! Reference source not found.**).

2.5.2 PSpice Simulations

A PSpice simulation was performed with a number of series capacitance values. The results with C_p = 0pF match the Simulink simulation very well while the C_p = 10pF showed a stable increase in the displacement to approximately 7µm. This could likely be increased by further adjusting the resistance used to tune the circuit. However, both simulation tools showed that the circuit produced the correct value for V_{act} in response to the value for C_{act}.

Table 2: Results of SIMULINK and PSpice Simulations

	Simulink	Simulink	Simulink	PSPICE1	PSPICE1	PSPICE2	PSPICE2	PSPICE2
x (um)	**Cact (pF)**	**Vint/n (V)**	**Vact (V)**	**Vin/n (V)**	**Vac (V)**	**Vin/n (V)**	**Vac (V)**	**Result**
0.00	7.2514	0	0	0	0.86	0	0.7534	stable
1.00	7.7474	3.4884	19.1425	-4.1955	-19.136	-4.07	-19.124	stable
2.00	8.3929	4.6255	23.6373	-5.27	-23.62	-5.18	-23.596	stable
3.00	9.2493	5.3354	24.987	-5.93	-24.976	-5.86	-24.971	stable
3.16	9.4119	5.4254	25.0118	-6.019	-25.001	-5.945	-24.995	stable
4.00	10.419	5.8223	24.4749	-6.35	-24.397	-6.283	-24.452	stable
5.00	12.086	6.1684	22.6263	-6.652	-22.636	-6.56	-22.645	stable
6.00	14.62	6.4159	19.7161	-6.812	-19.705	-6.713	-19.7	stable
7.00	18.884	6.5901	15.9084	-6.916	-15.899	-7.094	-16.704	stable
8.00	27.468	6.7069	11.3087	-6.957	-11.302	-6.8	-11.363	unstable
9.00	53.319	6.7774	5.9889	-6.9571	-5.9895	-6.5	-5.9816	unstable

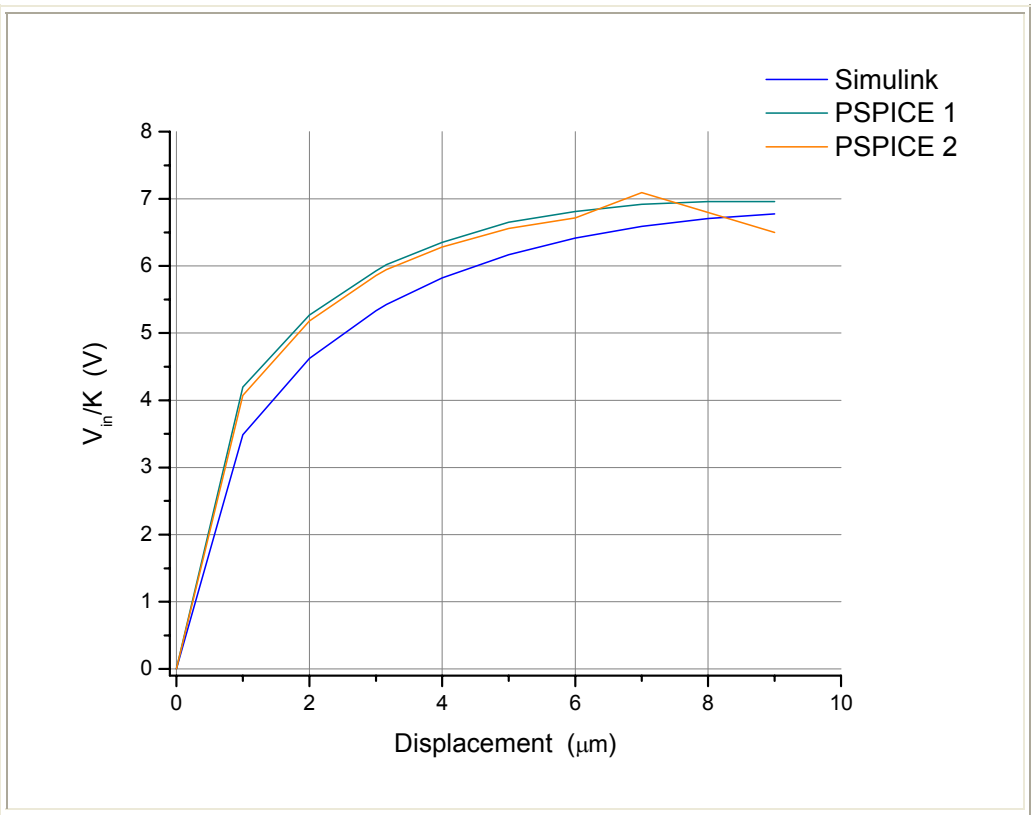

Figure 13: Plotted Results of Computer Simulations

) with all necessary attributes needed for testing the series capacitance method and synthetic voltage division controls. It was important to understand the contribution of the SVD and series capacitance methods. To that end, a simple implementation of a MEMS GCA design (**Error! Reference source not found.**) was used as a testbed. The test article was scaled upwards to a larger size (**Error! Reference source not found.**) in order to ensure precise manufacturing tolerances. This design is larger as compared to the original MEMSense design to accommodate the process selected for fabrication in the microelectronics laboratory at Auburn University.

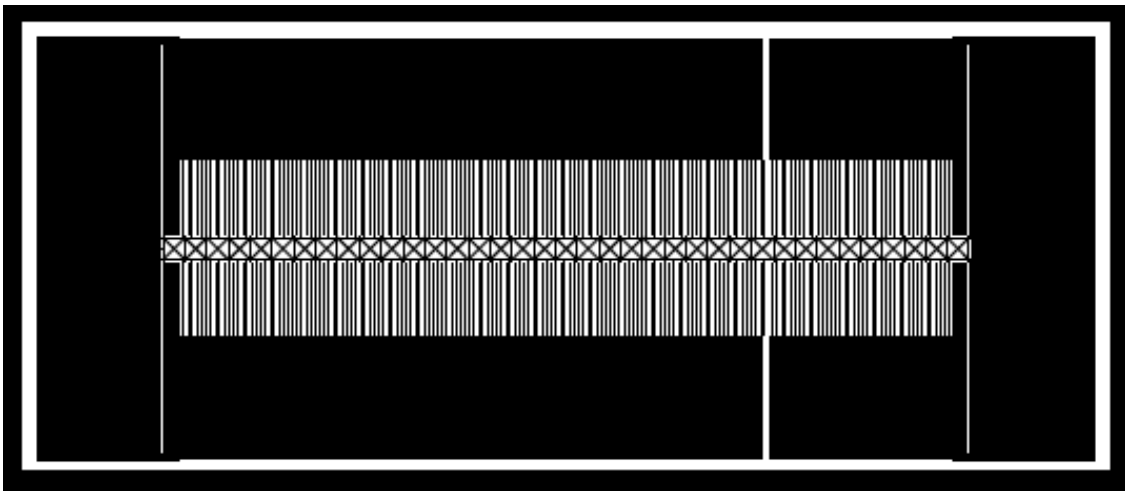

Figure 3: Layout of a single GCA Test Article

Multiple GCA elements were fabricated using a deep reactive-ion etching process (DRIE) using a single 100mm wafer composed of p-type crystalline silicon. The completed articles displayed the expected manufacturing precision for this process. Some images displaying detailed portions of the test article are found below in Figure 4 and Figure 5.

Table 1: GCA Test Article Features

Parameter	*Value*	*unit*
Comb length, l	600	µm
Comb width, g	10	µm
Inside Gap, x_1	10	µm
Outside Gap, x_2	25	µm
Comb teeth height, h	75	µm
Mass	3.6519×10^{-4}	kg
Damping constant	2.45×10^{-4}	N•s/m
Spring constant	103.125	N/m
Number of comb teeth	130	
ε_0	8.85×10^{-12}	F/m

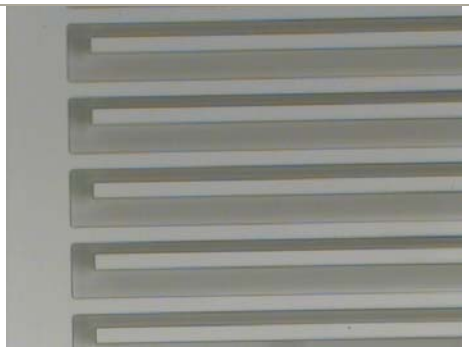

Figure 4: Image of the MEMS GCA Test Article Showing Comb Offsets

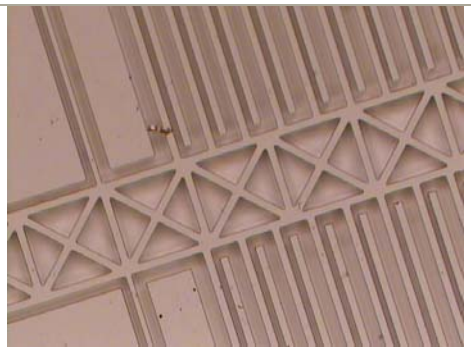

Figure 5: Image of MEMS GCA Test Article Showing the Central Beam Structure

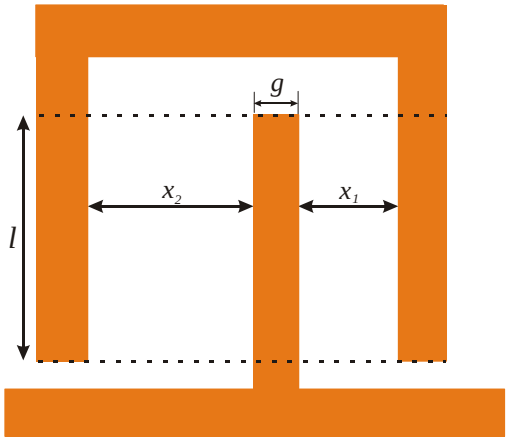

Figure 6: Detail of Interdigitated Combs

2.4 Synthetic Voltage Division to Enhance the Range of Motion

This system was modeled by a linear closed loop control system, as depicted in the block diagram in Figure 7.

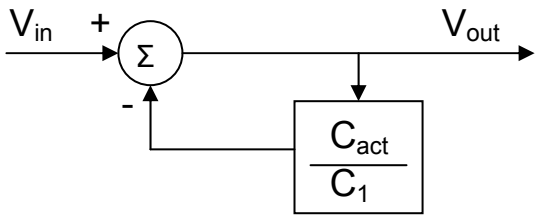

Figure 7: A Block Diagram Representation of the Series Capacitor Method

An important property of the linear control law representation is that all conceivable implementations of the system that can be modeled by the block diagram in Figure 7 can be used to generate V_{out} from V_{in}. By inserting a gain stage (Figure 8) in the forward path with a gain of n and increasing the series capacitor, C_1, by n, the input voltage can be reduced by n while still producing the same output voltage.

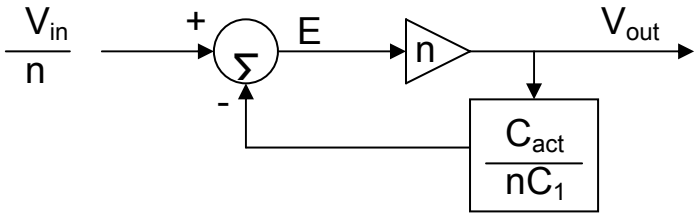

Figure 8: A Block Diagram of a Modified Series Capacitor Method Implementation

The key to realizing the controller illustrated in Figure 8 is a circuit that yields a voltage proportional to the ratio of the two capacitors, C_{act} and nC_1. However, this is a difficult ratio to realize. Consider the ideal charge amplifier circuit illustrated in Figure 9. Ideally, the output of this circuit is:

$$V_1 = -V_{act}\frac{C_{act}}{nC_s} \qquad \textbf{Eq. 1}$$

Using the charge amplifier, the controller modeled in Figure 8 was realized with the circuit in Figure 9. In this ideal circuit, the input voltage, V_{in}/n, is negative and the actuator drive voltage, V_{act}, is also negative. Since the actuator is a square law device where capacitance is proportional to V_{act}^2, the polarity of V_{act} does not matter. Therefore V_1 is greater than zero.

Figure 9: Ideal Charge Amplifier Circuit

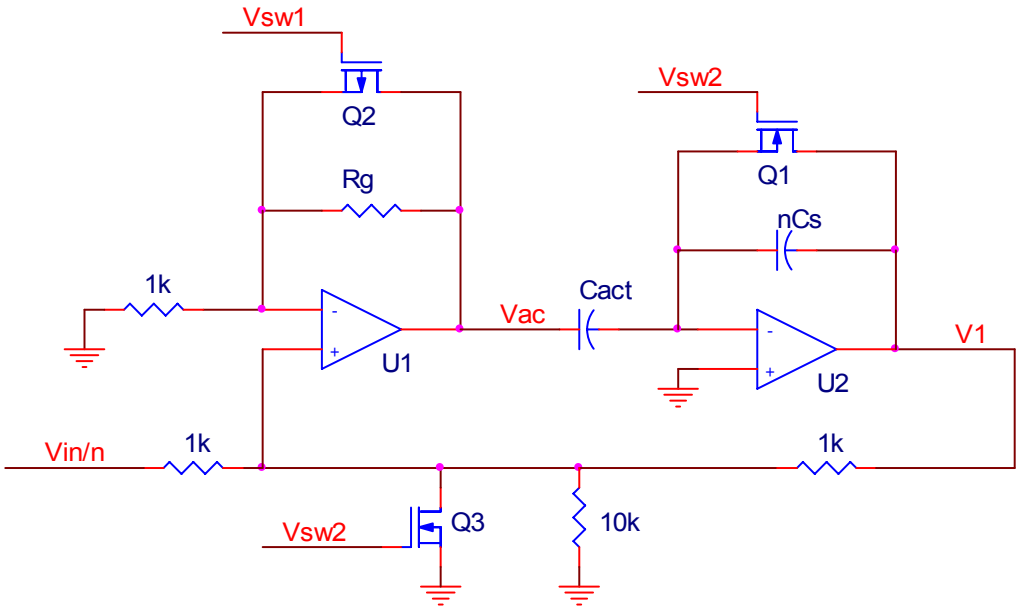

Figure 10: Realizable SVD Circuit

In order for the SVD controller to function correctly, if any parasitic or stray capacitance, C_p, is in parallel with the actuator, C_{act}, its effects must be canceled. Stray capacitance is cancelled via a tunable negation circuit (Figure 11).

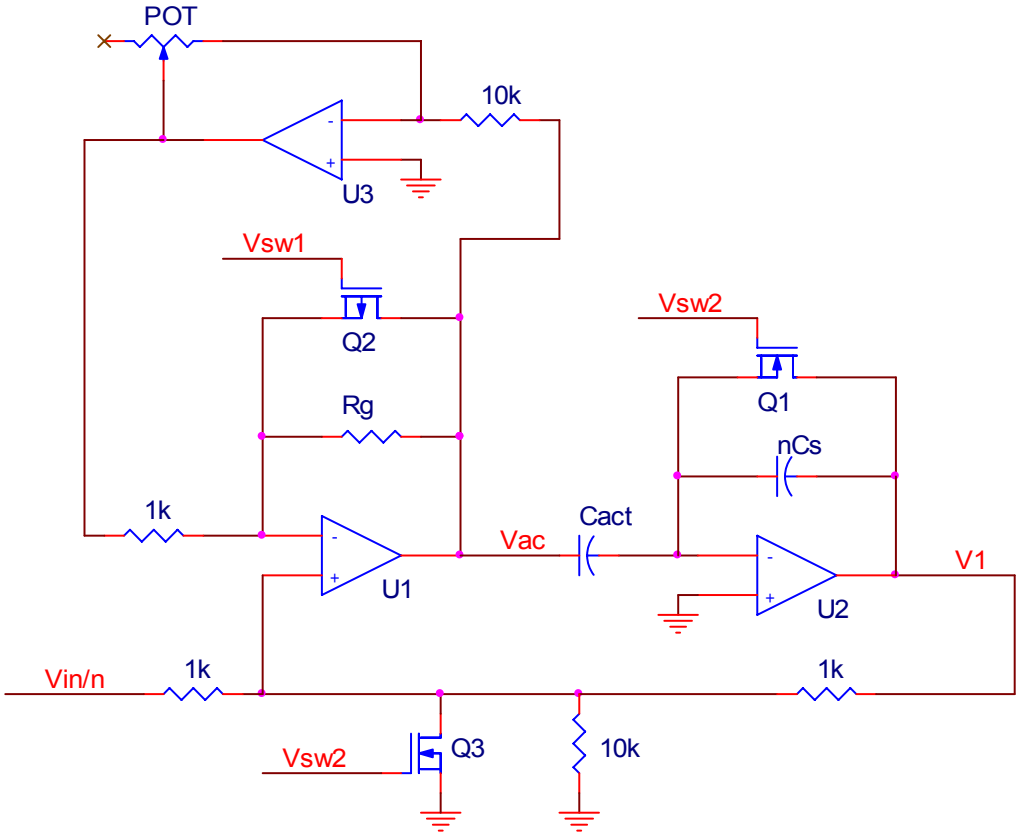

Figure 11: SVD controller Circuit with C_p Nulling.

2.5 Simulations

The GCA had a typical rectilinear layout with a larger number of comb fingers to ensure adequate signal strength for the evaluation of the series capacitance and SVD elements.

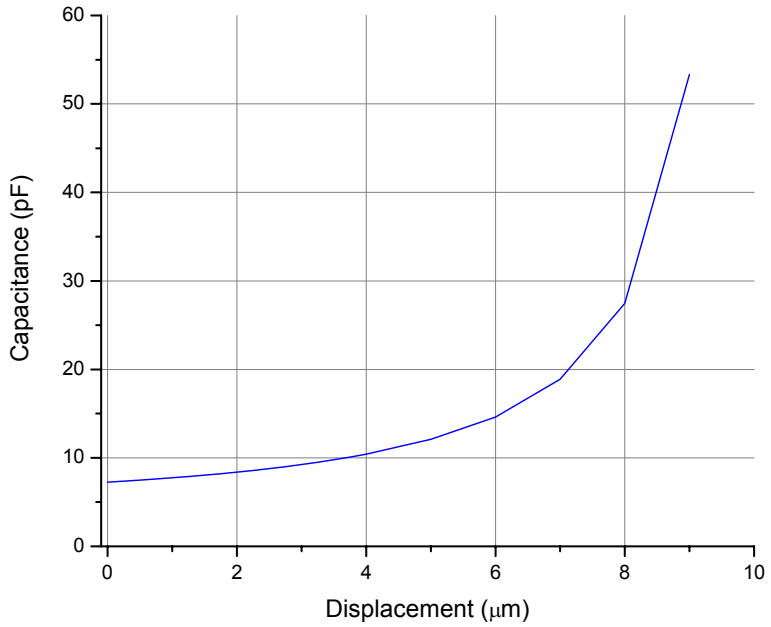

Figure 12: Capacitance vs. Displacement GCA Test Article

The computer simulations were performed while the SVD board and MEMS article were being fabricated. The solutions to the displacement vs. voltage calculations (**Error! Reference source not found.**) of the bare GCA displayed the highly nonlinear behavior that was expected from the design. Two models were developed one in the Simulink environment and another model in PSpice to test the combined GCA, series capacitance, and synthetic voltage division system.

2.5.1 Simulink Simulations

A simulation was conducted with a mathematical representation of the GCA with the addition of a series capacitance and the SVD controller. A nominal value of 1pF for the series capacitance, with a system gain K =48 for the controller, was chosen to establish a baseline response of the system. The resulting controller input voltage, V_{in} / K, and the resulting voltage across the actuator was determined for various values (**Error! Reference source not found.**).

2.5.2 PSpice Simulations

A PSpice simulation was performed with a number of series capacitance values. The results with C_p = 0pF match the Simulink simulation very well while the C_p = 10pF showed a stable increase in the displacement to approximately 7μm. This could likely be increased by further adjusting the resistance used to tune the circuit. However, both simulation tools showed that the circuit produced the correct value for V_{act} in response to the value for C_{act}.

Table 2: Results of SIMULINK and PSpice Simulations

	Simulink	Simulink	Simulink	PSPICE1	PSPICE1	PSPICE2	PSPICE2	PSPICE2
x (um)	**Cact (pF)**	**Vint/n (V)**	**Vact (V)**	**Vin/n (V)**	**Vac (V)**	**Vin/n (V)**	**Vac (V)**	**Result**
0.00	7.2514	0	0	0	0.86	0	0.7534	stable
1.00	7.7474	3.4884	19.1425	-4.1955	-19.136	-4.07	-19.124	stable
2.00	8.3929	4.6255	23.6373	-5.27	-23.62	-5.18	-23.596	stable
3.00	9.2493	5.3354	24.987	-5.93	-24.976	-5.86	-24.971	stable
3.16	9.4119	5.4254	25.0118	-6.019	-25.001	-5.945	-24.995	stable
4.00	10.419	5.8223	24.4749	-6.35	-24.397	-6.283	-24.452	stable
5.00	12.086	6.1684	22.6263	-6.652	-22.636	-6.56	-22.645	stable
6.00	14.62	6.4159	19.7161	-6.812	-19.705	-6.713	-19.7	stable
7.00	18.884	6.5901	15.9084	-6.916	-15.899	-7.094	-16.704	stable
8.00	27.468	6.7069	11.3087	-6.957	-11.302	-6.8	-11.363	unstable
9.00	53.319	6.7774	5.9889	-6.9571	-5.9895	-6.5	-5.9816	unstable

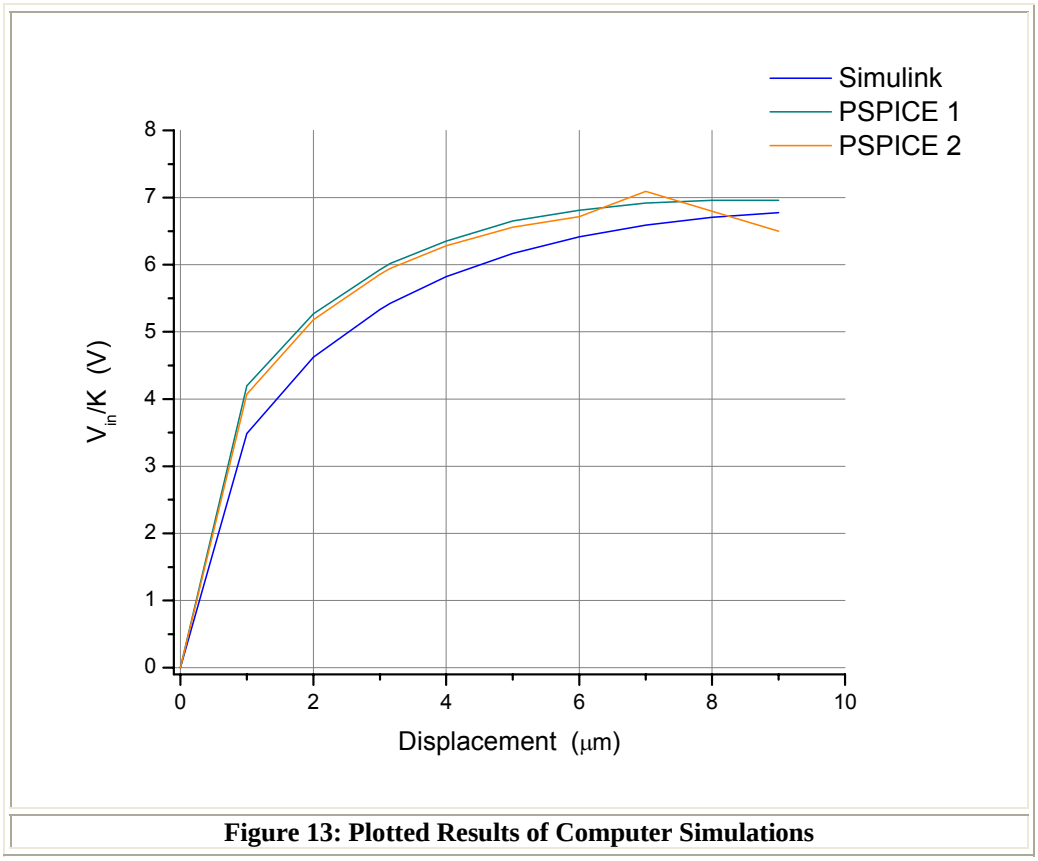

Figure 13: Plotted Results of Computer Simulations

2.6 *Test Method and Evaluation of the Control Methods*

The SVD controller board was fabricated using a two layer layout and was populated. For evaluating the SVD controller board, a separate capacitor test board was designed and fabricated as well. The capacitor test board consisted of 20 surface mount (1206 size) 150pF capacitors in series, where the capacitance could be probed anywhere along the chain of capacitors.

Table 3 lists the designed and measured capacitance values for the capacitor test board. A photograph of the fabricated and populated capacitor test board is shown in Figure 15.

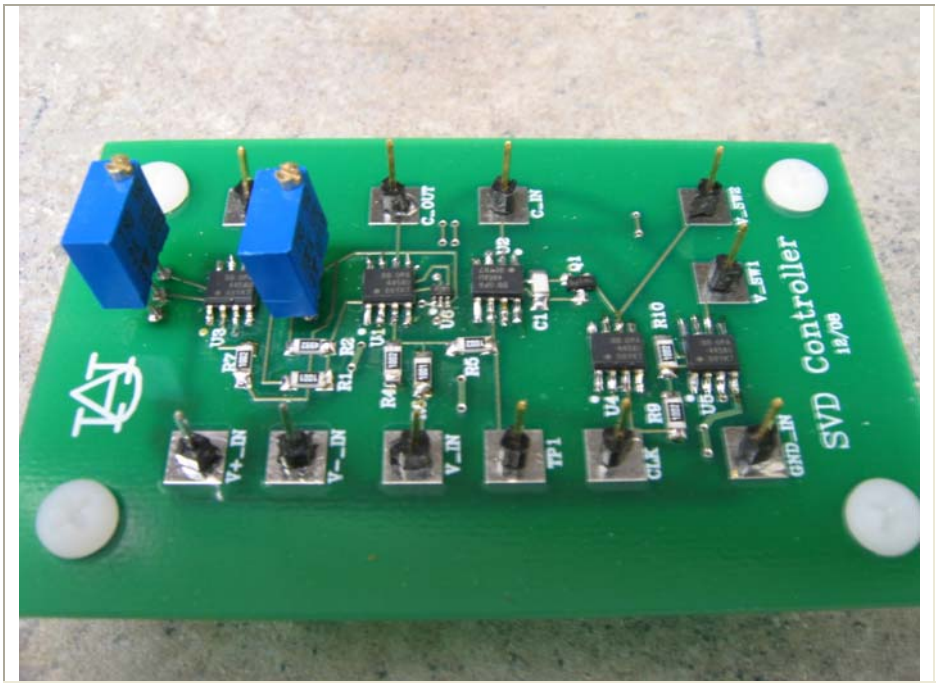

Figure 14: The SVD Controller Board

Table 3: Capacitance Values for the Capacitor Test Board.

	C (pF)	C (pF)	C (pF)	C (pF)
Pin	designed	120 Hz	1 kHz	10 kHz
C	150	150	148	147.4
C/2	75	78	76.3	76.3
C/3	50	54	51.5	51.5

C/4	37.5	40	39.4	39
C/5	30	33	32	31.5
C/6	25	28	26.6	26.61
C/7	21.43	24	23	23.02
C/8	18.75	22	20.8	20.41
C/9	16.67	20	18.6	18.32
C/10	15	18	16.8	16.69
C/11	13.64	17	15.5	15.28
C/12	12.5	16	14.6	14.2
C/13	11.54	15	13.1	13.14
C/14	10.71	14	12.5	12.41
C/15	10	13	12	11.56
C/16	9.38	12	11.1	10.99
C/17	8.82	12	10.4	10.33
C/18	8.33	11	11.2	9.97
C/19	7.89	10	9.8	9.42
C/20	7.5	10	9.3	9.06

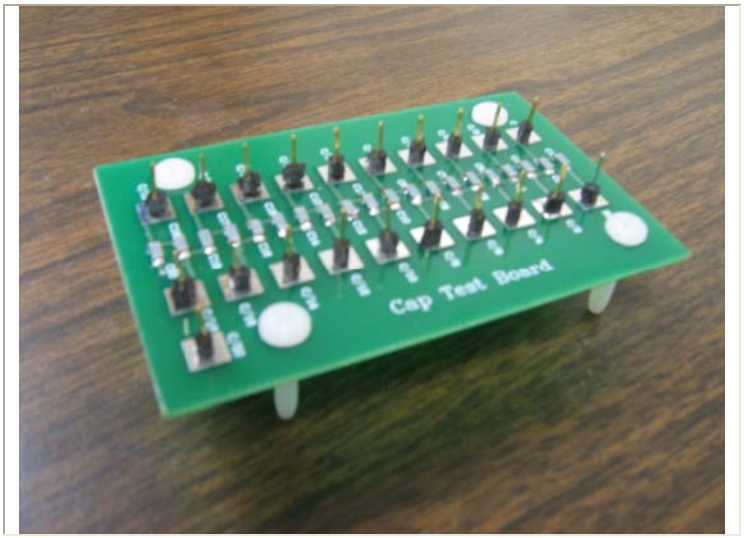

Figure 15: Capacitor Test Board

The values on the capacitance test board were measured and used for calculations comparing the laboratory system to the computer simulations. The measured capacitance values were correlated with the estimated Simulink modeled GCA capacitances with added stray or parasitic capacitance, as shown in Table 3. Then, based on the Simulink results, values for the SVD controller input voltage V_{in}/N and the actuator drive voltage, V_a were estimated. The SVD controller was connected to the capacitor test board using jumper cables and was then powered with approximately ±41.7V using 60V adjustable power supplies (BK Precision 1667). A third adjustable

power supply (Agilent E3631A) was used to provide the input voltage to the SVD controller board. A 5MHz function generator (BK Precision 4011A) was used to provide the 5V clock signal to the board at approximately 43KHz, with an 11% duty cycle which is the minimum possible with this source. Data was collected using an Agilent DSO3202A digital storage scope. To test the SVD controller board, the various capacitor values were used while adjusting the input voltage to the board. If the board response was not correct, the two potentiometers on the board were adjusted to adjust the loop gain of the controller and the parasitic capacitance nulling circuit. After several iterations of this process, data was collected (shown in Table 3).

Table 3: SVD Controller Board Evaluation Data

			Estimate	Estimate	Measured	Measured
Meas	C (pF)	C (no Cpar)	Vin/N	Va	Vin/N	Va
C	147.4	145.5914				
C/2	76.3	74.4914	-6.78	-4	-0.56	-4
C/3	51.5	49.6914	-6.75	-6.2	-0.571	-6
C/4	39	37.1914	-6.73	-8	-0.605	-8
C/5	31.5	29.6914	-6.71	-10.5	-0.642	-10.5
C/6	26.61	24.8014	-6.65	-12.5	-0.637	-12.5
C/7	23.02	21.2114	-6.6	-14	-0.625	-14
C/8	20.41	18.6014	-6.55	-16.1	-0.619	-16
C/9	18.32	16.5114	-6.49	-17	-0.603	-17
C/10	16.69	14.8814	-6.42	-19	-0.602	-19
C/11	15.28	13.4714	-6.3	-20	-0.583	-20
C/12	14.2	12.3914	-6.2	-21	-0.574	-21
C/13	13.14	11.3314	-6	-23.8	-0.592	-23.5
C/14	12.41	10.6014	-5.9	-24.2	-0.561	-24
C/15	11.56	9.7514	-5.5	-24.8	-0.552	-25
C/16	10.99	9.1814	-5	-24.2	-0.513	-24.5
C/17	10.33	8.5214	-4.8	-23.9	-0.475	-24
C/18	9.97	8.1614	-4.5	-23.5	-0.45	-23.5
C/19	9.42	7.6114	-4.4	-19.1	-0.348	-19
C/20	9.06	7.2514	0	0	0	0

The SVD system was found to be stable over a wide range of actuator displacement. This is the most important factor in the experimental evaluation of the SVD system

which clearly defines the success of the method. The system contains a number of components that can introduce instabilities including the charge amplifier, the feedback controller and the stray capacitance nulling loop. The successful operation of a stable system lends credence to each element's stability. The measured voltage per unit gain, Vin/K, was much smaller than was found in the estimates. This is most likely due to a higher system gain constant, K, than was modeled, which may have resulted from the charge amplifier's gain capacitance being smaller than expected. The controller output voltage, Va, did not display the exact response expected, but the observed response may be considered to be within the variances inherent in component tolerances to judge the system a success. Some contributions to the difference observed between ideal values obtained from the models and the laboratory trials may involve unaccounted stray capacitance present in the system. It may also be possible that the system gain lies outside of the tuning range of the variable resistors used in the circuit and therefore the circuit is slightly mistuned. Since both potentiometers must be tuned to the correct values for perfect operation, the operator is presented with a two-dimensional tuning problem. The tuning capability is currently being revised to allow better control. The successful application of the SVD has been thoroughly established by these trials and the models validated by the data collected to date.

3.0 Commercialization

3.1. *Strong Growth in MEMS Gyroscopes*

MEMS gyro revenues have shown very strong growth in sales with the automotive industry comprising a significant portion of the market. The automotive market alone has been forecast to grow at a compounded growth rate of 11.2% per year with unit sales increasing by 14.4% per year in the coming years (Table 4). Defense and aerospace account for the remaining market share. MEMSense's diverse customer base reflects these demographics.

Table 4: MEMS Gyroscope Revenue Forecast, [1]

	2008	2009	2010	2011	2012
Revenues (*millions*)	$621.0	$762	$721.9	$1063.7	$1275.1
Growth Rate[†]	11.6	9.1	9.5	6.2	6.9

[†]*Growth rate reflects the automotive segment*

3.2 *Competition and Potential for Market Share*

Analog Devices markets the ADXRS gyro which is currently utilized in MEMSense products. The ADXRS is a rate gyro that sells for $40 in single-unit quantities and $29 in 100k quantities. The ADXRS long-term bias drift is on the order of 100 º/hr, making it very difficult to utilize in many sensing applications, thereby limiting it to less demanding applications. The deficiencies are even more apparent when these device are

incorporated into heading systems that numerically integrate the angular rate output of these gyros. Significant size and power requirements are added to these systems in the form of digital processing , thwarting efforts by designers to minimize the overall size and power needs of the system. The best performing gyro on the market today is the BEI Technologies QRS11. The long-term drift for the QRS11 is 30 º/hr. This gyro has a single unit sales price of $1400, and 1000 unit pricing of approximately $1000 displaying the high cost associated with higher precision devices existing in today's market. The MEMSense gyroscopes using SVD and series capacitance elements are based on completely different concepts than the current state of-the-art MEMS gyroscopes. A high performance gyroscope such as those developed by MEMSense have the ability to compete in the world sensors market aggressively both in cost and miniaturization.

4.0 Remaining Problems and Unfulfilled Research Objectives

The models did not match the laboratory trials exactly and it has been left to determine what mechanisms cause the deviations that were encountered. Work will continue towards resolving these questions. Some determination as to the cost associated with implementing the SVD controller and series capacitance methods in a CMOS chip that already includes the various systems used to operate the gyros has not occurred yet, but is planned in the near future. This work will wrap up any remaining questions regarding the pricing of the MEMSense gyroscope as a result of implementing the SVD and series capacitance methods. Most aspects of the Phase I were pursued or accomplished as detailed in the original task list in the allotted time. Some avenues for further research were realized and it is the intention of the investigators involved to pursue funding in the form of a Phase II in order to fully realize the potential of this technology as applied to MEMS inertial sensors Their remains great potential for a highly competitive gyroscope to result from the application of the discussed methods.

5.0 Conclusions

The series capacitance method and the synthetic voltage division methods will both lend benefits to GCA design, especially for designs in current development by MEMSense. These methods mesh well with the MEMS devices being designed today that in the future will measure angular displacement directly as opposed to current gyroscope technologies that output signals proportional to angular rate alone. The next generation of inertial measurement units, comprised of three-axis acceleration measurement and

angular measurement will perform better than current inertial measurement technology, especially in the application to heading sensor systems. Current heading technology that utilizes MEMS sensors suffer large detrimental noise amplitudes that are further exacerbated by numerical integration of the attitude signals, themselves characterized by large white noise amplitudes. Heading determination based solely on the reckoning provided by MEMS based devices is currently not comparable to the precision found in more traditional technologies. The experience of the MEMSense staff with numerous customers in the automotive, defense and aerospace domains leads to the conclusion that there is very significant demand for IMU information in smaller, and more precise forms. The implementation of the series capacitance method and the synthetic voltage division methods to a MEMSense absolute angle MEMS gyroscope will open the door to miniature precision inertial measurement units and more sophisticated applications in which they are employed.

6.0 References

[1] Frost & Sullivan, *World MEMS Sensors Markets*, #FA0A-32, Frost & Sullivan, 2006.

Appendix A: SVD Controller Schematic

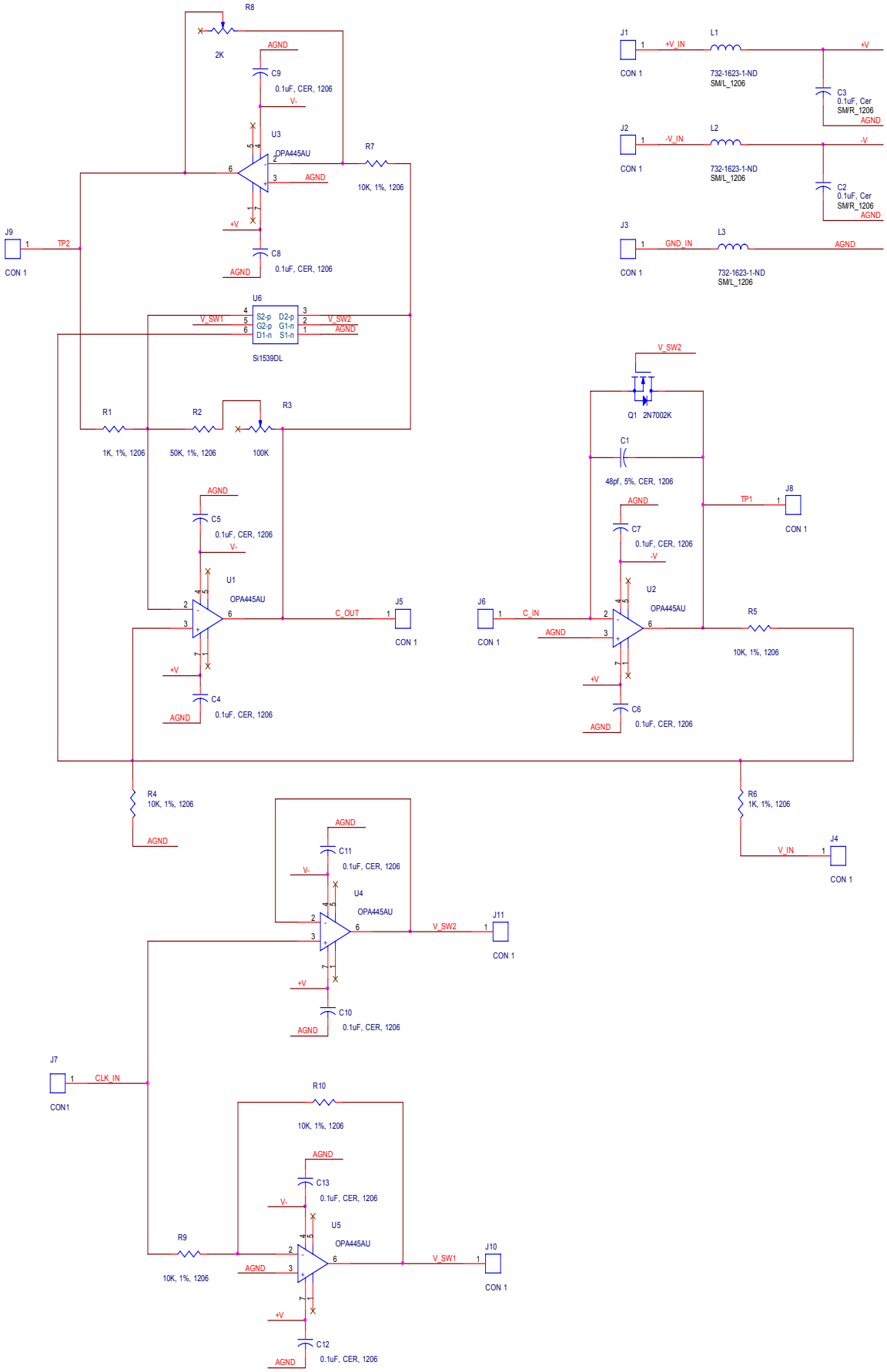
R8
2K
AGND
C9
0.1uF, CER, 1206
V-
U3
OPA445AU
R7
10K, 1%, 1206
+V
C8
0.1uF, CER, 1206
J9
TP2
CON 1
U6
V_SW1
V_SW2
Si1539DL
R1
1K, 1%, 1206
R2
50K, 1%, 1206
R3
100K
C5
0.1uF, CER, 1206
U1
OPA445AU
C_OUT
J5
CON 1
C4
0.1uF, CER, 1206
J1
+V_IN
L1
732-1623-1-ND
SM/L_1206
+V
C3
0.1uF, Cer
SMR_1206
J2
-V_IN
-V
C2
0.1uF, Cer
SMR_1206
J3
GND_IN
L3
V_SW2
Q1 2N7002K
C1
48pf, 5%, CER, 1206
J8
TP1
C7
0.1uF, CER, 1206
U2
OPA445AU
J6
C_IN
R5
10K, 1%, 1206
C6
0.1uF, CER, 1206
R4
10K, 1%, 1206
R6
1K, 1%, 1206
V_IN
J4
C11
0.1uF, CER, 1206
U4
OPA445AU
V_SW2
J11
C10
0.1uF, CER, 1206
J7
CLK_IN
CON1
R10
10K, 1%, 1206
C13
0.1uF, CER, 1206
U5
OPA445AU
R9
10K, 1%, 1206
V_SW1
J10
C12
0.1uF, CER, 1206